Original Article

JCBFM

Journal of Cerebral Blood Flow & Metabolism
2018, Vol. 38(4) 659–668
© Author(s) 2017
Reprints and permissions:
sagepub.co.uk/journalsPermissions.nav
DOI: 10.1177/0271678X17746179
journals.sagepub.com/home/jcbfm
SAGE

The importance of small polar radiometabolites in molecular neuroimaging: A PET study with [^{11}C]Cimbi-36 labeled in two positions

Annette Johansen[1,2], Hanne D Hansen[1], Claus Svarer[1], Szabolcs Lehel[3], Sebastian Leth-Petersen[4], Jesper L Kristensen[4], Nic Gillings[3] and Gitte M Knudsen[1,2]

Abstract

[^{11}C]Cimbi-36, a 5-HT$_{2A}$ receptor agonist PET radioligand, contains three methoxy groups amenable to [^{11}C]-labeling. In pigs, [^{11}C]Cimbi-36 yields a polar (M1) and a less polar (M2) radiometabolite fraction, while changing the labeling to [^{11}C]Cimbi-36_5 yields only the M1 fraction. We investigate whether changing the labeling position of [^{11}C]Cimbi-36 eliminates M2 in humans, and if this changes the signal-to-background ratio. Six healthy volunteers each underwent two dynamic PET scans; after injection of [^{11}C]Cimbi-36, both the M1 and M2 fraction appeared in plasma, whereas only the M1 appeared after [^{11}C]Cimbi-36_5 injection. [^{11}C]Cimbi-36_5 generated higher uptake than [^{11}C]Cimbi-36 in both neocortex and cerebellum. With the simplified reference tissue model mean neocortical non-displaceable binding potential for [^{11}C]Cimbi-36 was 1.38 ± 0.07, whereas for [^{11}C]Cimbi-36_5, it was 1.18 ± 0.14. This significant difference can be explained by higher non-displaceable binding caused by demethylation products in the M1 fraction such as [^{11}C]formaldehyde and/or [^{11}C]carbon dioxide/bicarbonate. Although often considered without any impact on binding measures, we show that small polar radiometabolites can substantially decrease the signal-to-background ratio of PET radioligands for neuroimaging. Further, we find that [^{11}C]Cimbi-36 has a better signal-to-background ratio than [^{11}C]Cimbi-36_5, and thus will be more sensitive to changes in 5-HT$_{2A}$ receptor levels in the brain.

Keywords

[^{11}C]Cimbi-36, 5-HT$_{2A}$ receptor, labeling position, positron emission tomography, polar radiometabolites

Received 28 July 2017; Accepted 25 October 2017

Introduction

Developing tracers for positron emission tomography (PET) imaging is very challenging because of the many criteria that have to be met, particularly for targets located in the brain.[1,2] As is the case for central nervous system (CNS) drug development in general, many compounds are discarded as radioligands because they fail in in vitro, in vivo preclinical or clinical experiments. One of the most frequent reasons for failure of a radioligand is when an insufficient target to background ratio emerges, i.e. when the non-displaceable binding in the brain exceeds the target binding. Disproportionally high non-displaceable brain binding is often ascribed to high non-specific binding to, e.g. lipids or proteins. Radiolabeled metabolites can also be the cause of non-displaceable binding, but the general notion[1,3] is that as long as radiometabolites are polar, they do not cross the blood–brain barrier (BBB) and thus one does not need to worry about them binding either

[1]Neurobiology Research Unit and Center for Integrated Molecular Brain Imaging, Rigshospitalet, Copenhagen, Denmark
[2]Faculty of Health and Medical Sciences, University of Copenhagen, Copenhagen, Denmark
[3]PET & Cyclotron Unit, Rigshospitalet, Copenhagen, Denmark
[4]Department of Drug Design and Pharmacology, Faculty of Health and Medical Sciences, University of Copenhagen, Copenhagen, Denmark

Corresponding author:
Gitte M Knudsen, Copenhagen University Hospital, Rigshospitalet, Section 6931, 9 Blegdamsvej, Copenhagen DK-2100 O, Denmark.
Email: gitte@nru.dk ORCID

specifically or non-specifically to targets within the brain. Radiometabolites considered too polar to enter the brain are rarely identified and here, ''polar enough'' often means that they clearly separate from the more lipophilic parent compound on radio-high performance liquid chromatography (HPLC).

Systemic injection of [^{11}C]Cimbi-36, a newly developed serotonin 2A (5-HT$_{2A}$) receptor agonist PET tracer, leads to two separated radiometabolite fractions identified in both pigs[4] and humans.[5] One fraction, M1, is considered to be highly polar, as it has short retention time on the HPLC column. The other fraction, M2, is considered to be more lipophilic, as it has a longer retention time. These terms, however, merely refer to their lipophilicity relative to each other and to the parent compound. After injection of [^{11}C]Cimbi-36, Ettrup et al.[4] did not find any radiometabolites in pig brain homogenate, at least not to an extent that would interfere with the PET signal from [^{11}C]Cimbi-36 itself. When [^{11}C]Cimbi-36 was evaluated in humans, the total distribution volume (V_T) of the reference region (cerebellum) decreased by 3% when the scan time was truncated to 60 min compared with the full scan time of 120 min, possibly because of radiometabolites accumulating in the brain.[5]

Metabolism of radiotracers is often not investigated in detail, but case reports show that when taken as a recreational drug, Cimbi-36 may be associated with severe toxicity[6] and consequently, its metabolism has been thoroughly investigated. Leth-Petersen et al.[7] showed that demethylation of Cimbi-36 takes place in both pig and human liver microsomes. In vivo this is followed by rapid conjugation to glucuronic acid, which is a common phase II metabolic route. The M2 radiometabolite fraction was thus identified as a radiolabeled glucuronide conjugate (predominately at the 5'-position), while the M1 fraction results from cleavage of the [^{11}C]-methyl group in the methoxybenzyl moiety of [^{11}C]Cimbi-36.

[^{11}C]Cimbi-36 is an interesting radioligand because it is amenable to radiolabeling at three different positions (Figure 1). In pigs, changing the labeling position from the 2-methoxybenzyl-position ([^{11}C]Cimbi-36, Figure 1(a)) to the 5′-methoxy-4-bromophenethylamine position ([^{11}C]Cimbi-36_5, Figure 1(b)) eliminates the presence of the M2 fraction, leaving only the M1 fraction, as a result of demethylation of the 5′-*O*-methyl group.[7] Aside from being polar, the specific identity and characteristics of the M1 fraction are still unknown, while the nature of the glucuronide conjugate (M2 fraction) makes it unlikely to easily cross the BBB, although previous studies were not fully conclusive.[4,5] Therefore, we wished to investigate (1) whether changing the labeling position of [^{11}C]Cimbi-36 to that of [^{11}C]Cimbi-36_5 would eliminate the M2 radiometabolite fraction in human plasma, and (2) if this would change the signal-to-background ratio in the brain, thus evaluating whether [^{11}C]Cimbi-36 radiometabolites do in fact enter the brain.

Materials and methods

Study design

Eight female healthy volunteers (mean age ± SD; 23.6 ± 3.1 years) were included in the study. Preliminary plasma radiometabolite data from three of the subjects have previously been described.[7] The study was approved by the ethics committee for the Capital Region of Denmark (protocol KF-01-2008), conducted in accordance with declaration of Helsinki, and all participants signed an informed consent form. Six of the subjects completed two full PET scans; [^{11}C]Cimbi-36 labeled in one of two different positions was injected. For technical reasons, one subject did not complete the [^{11}C]Cimbi-36 scan, but blood samples were obtained, while another subject underwent the [^{11}C]Cimbi-36 scan only.

We scanned with the high-resolution research tomography (HRRT) PET scanner (CTI/Siemens, Knoxville, TN, USA), after an antecubital vein bolus injection of radiotracer. [^{11}C]Cimbi-36 (467 ± 101 MBq, 0.33 ± 0.19 μg, 789 ± 405 GBq/μmol, $n = 8$) and [^{11}C]Cimbi-36_5 (546 ± 64 MBq, 0.31 ± 0.10 μg, 737 ± 275 GBq/μmol, $n = 7$) were produced as described by Leth-Petersen et al.[7] Dynamic 120 min PET scanning started at the time of injection. Two subjects had the [^{11}C]Cimbi-36 scan before the [^{11}C]Cimbi-36_5 scan, while the order was reversed for the remaining subjects. The intervals between first and second scans were 2.7 h, 2.8 h, 3.0 h, 3.1 h, 4.8 h, 14 days, and 30 days.

To determine the radiometabolite profiles of the radiotracers with radio-HPLC, and to measure radioactivity in plasma and whole blood, venous blood samples were manually drawn ($t = 1$, 5, 10, 20, 30, 45, 60, 90, 120 min) from a catheter in the opposite cubital vein.

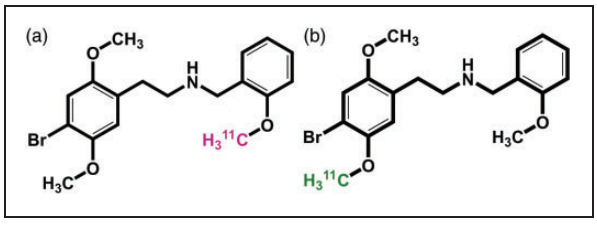

Figure 1. Chemical structures and labeling position of [^{11}C]Cimbi-36 (a) and [^{11}C]Cimbi-36_5 (b). ([^{11}C]Cimbi-36_2 not shown).

Positron emission tomography quantification

Reconstruction of PET images was done as previously described[8] by sorting data into 45 dynamic frames (6×10 s, 6×20 s, 6×60 s, 8×120 s, 19×300 s). For subject 2, median intra-scan motion of the [^{11}C]Cimbi-36_5 scan was more than 3 mm, and all frames were therefore aligned to the first 5 min frame using the AIR software (Automated Image Registration, v. 5.2.5, LONI, UCLA, http://bishopw.loni.ucla.edu/air5/).

Predefined regions of interest (ROIs) were automatically delineated based on the subject's T1-weighted MR image, and used to generate time-activity curves (kBq/mL) as previously described.[5] Neocortex was constructed as a volume-weighted region of the following cortical regions: orbitofrontal cortex, medial inferior gyrus, anterior cingulate cortex, insula, superior temporal gyrus, parietal cortex, medial inferior temporal gyrus, superior frontal gyrus, occipital cortex, sensory-motor cortex, posterior cingulate cortex, dorsolateral prefrontal gyrus, ventrolateral prefrontal gyrus. In addition, thalamus, putamen and caudate nucleus were analyzed. From these, standardized uptake values (SUV; g/mL) were calculated by normalizing to injected dose per bodyweight (kBq/g). Non-displaceable binding potentials (BP_{ND}s) for the abovementioned ROIs were calculated in PMOD version 3.0 (PMOD Technologies Ltd, Zürich, Switzerland), using the simplified reference tissue model (SRTM)[5] with cerebellum (without vermis[9]) as reference tissue. Regions with a coefficient of variance (COV) above 10% for the BP_{ND} estimate were excluded from the analysis. This was the case for the following regions in all but two scans: entorhinal cortex, hippocampus, amygdala, hypothalamus, as well as a few of the cortical subregions (see Table 1.)

Radiometabolite analysis

Venous blood samples were analyzed using a column-switching HPLC system as previously described,[10] but with some modifications. Briefly, plasma samples were obtained from blood samples by centrifugation, mixed 1:1 with pH 7.2 HPLC eluent (see below) and filtered using 0.45 μm syringe filter prior to HPLC analysis (Ultimate 3000 system, Thermo Scientific) with an in-line radiodetector (Posi-RAM, LabLogic, UK). Extraction of the lipophilic component of the plasma was achieved using a Shim-pack MAYI-ODS(G) column (30×4.6 mm, 50 μm particles, Shimadzu) with a mobile phase consisting of 20 mM sodium dihydrogen phosphate and 2 mM sodium-1-decane sulphonate (adjusted to pH 7.2 with phosphoric acid) and 2% 2-propanol at a flow rate of 5 mL/min. After a 4-min extraction step, the extraction column was eluted (reverse flow direction) with 30% acetonitrile in 100 mM disodium hydrogen phosphate (pH 2.6), containing 5 mM sodium-1-decane sulphonate, flow rate 5 mL/min, through an analytical column (Onyx Monolithic C-18, 50×4.6 mm, Phenomenex Aps, Denmark). The total analysis time was 8 min per sample and up to 2 mL plasma could be analyzed per injection.

Parent and metabolite fractions were quantified as previously described.[5] Plasma and whole blood radioactivity were measured using a well counter (Cobra 5003; Packard Instruments, Meriden, CT, USA) that was cross-calibrated to the HRRT scanner. Radioactivity counts were decay corrected to time of injection for all samples.

Statistical analysis

All statistical analyzes were performed with GraphPad Prism (version 7.01, GraphPad Software, Inc., CA, USA). All values are given as mean ± SD unless otherwise noted. P values below 0.05 were considered significant.

Results

Kinetic modeling

Analysis of the time-activity curves for the six subjects that completed full PET scans with both radioligands showed that injection of [^{11}C]Cimbi-36_5 resulted in higher standardized uptake values (SUVs) than did [^{11}C]Cimbi-36: the mean peak SUVs were 4.2 ± 0.4 g/mL versus 3.8 ± 0.9 g/mL for the high-binding region (neocortex) and 3.1 ± 0.3 g/mL versus 2.9 ± 0.9 g/mL for cerebellum (Figure 2(a)). The standard deviations for the time-activity curves were notably higher for [^{11}C]Cimbi-36_5. The mean time to peak in the neocortex was shorter for [^{11}C]Cimbi-36 as compared to [^{11}C]Cimbi-36_5 (47 ± 19 min versus 64 ± 13 min, paired t-test, $p < 0.05$). Kinetic modeling using the SRTM, with cerebellum as reference tissue, resulted in a higher mean neocortical BP_{ND} for [^{11}C]Cimbi-36 compared with [^{11}C]Cimbi-36_5 (1.38 ± 0.07 versus 1.18 ± 0.14, paired t-test, $p = 0.0026$, $n = 6$). The difference in SUV and BP_{ND} is visible on a single subject basis (Figure 2(b) to (e)).

Because neocortex is a weighted average of multiple cortical regions, we investigated whether this difference was driven by any particular cortical region(s), which was not the case, as seen in Table 1. We found a

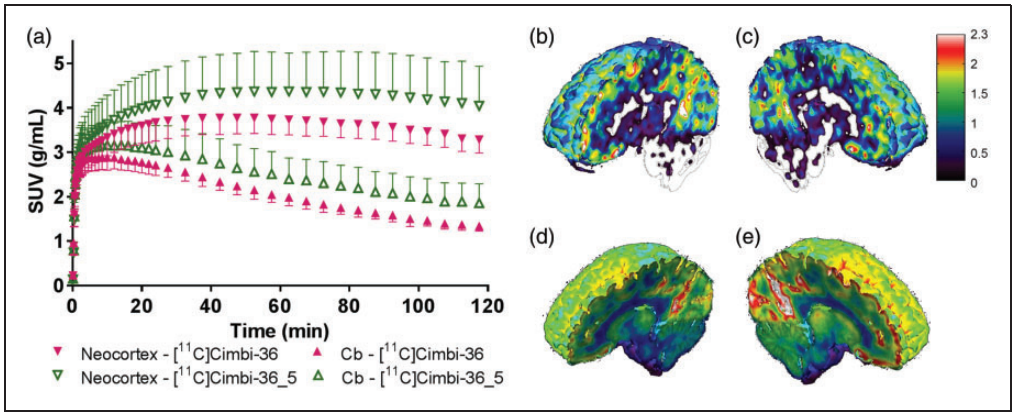

Figure 2. (a) Standard uptake values (SUV) in neocortex and cerebellum (Cb) for [^{11}C]Cimbi-36 and [^{11}C]Cimbi-36_5 (points represent mean ± SD, $n = 6$). On the right: Maps of BP_{ND} (b and c) and corresponding SUV images (d and e) in one subject scanned with [^{11}C]Cimbi-36 (b, d) and [^{11}C]Cimbi-36_5 (c, e).

Table 1. Difference in BP_{ND} calculated with the SRTM for [^{11}C]Cimbi-36 and [^{11}C]Cimbi-36_5.

	[^{11}C]Cimbi-36			[^{11}C]Cimbi-36_5			Mean difference[a]	
	Mean	SD	*N*	Mean	SD	*N*	Absolute	%
Anterior cingulate gyrus	1.73	0.24	5	1.37	0.21	6	0.32	20.5
Dorsolateral prefrontal gyrus	1.39	0.15	6	1.30	0.19	6	0.09	6.8
Insula	1.59	0.22	5	1.38	0.22	6	0.21	14.4
Medial inferior frontal gyrus	1.42	0.11	6	1.24	0.18	6	0.17	13.5
Medial inferior temporal gyrus	1.49	0.14	6	1.21	0.13	6	0.29	21.4
Occipital cortex	1.24	0.10	6	1.07	0.11	6	0.17	14.6
Orbito frontal cortex	1.66	0.22	6	1.23	0.25	6	0.43	30.4
Parietal cortex	1.48	0.11	6	1.23	0.19	6	0.25	19.1
Posterior cingulate cortex	1.40	0.09	6	1.16	0.14	6	0.24	19.2
Sensory motor cortex	1.07	0.14	5	0.95	0.18	6	0.14	14.7
Superior frontal gyrus	1.34	0.09	6	1.20	0.17	6	0.14	11.8
Superior temporal gyrus	1.57	0.12	6	1.32	0.13	6	0.25	17.7
Ventrolateral prefrontal cortex	1.45	0.16	6	1.23	0.19	6	0.22	17.1
Caudate nucleus	0.31	0.05	5	0.27	0.08	5	0.04	14.7
Putamen	0.37	0.03	4	0.30	0.09	5	0.05	16.0
Thalamus	0.38	0.08	4	0.37	0.06	5	0.03	5.9

[a]Only paired measurements are included.

significant correlation between regional BP_{ND} values measured with [^{11}C]Cimbi-36 and [^{11}C]Cimbi-36_5 for all subjects, based on both high-binding (neocortical) and low-binding regions (thalamus, putamen, caudate nucleus), with a mean $R^2 = 0.89$ ($n = 6$). Linear regression of BP_{ND} values for all subjects yielded the following equation: $0.77X + 0.072$ (with [^{11}C]Cimbi-36 as the independent variable and [^{11}C]Cimbi-36_5 as the dependent variable), and the slope was significantly different from 1 ($p < 0.0001$, $R^2 = 0.88$). When the slope was forced through the origin, the regression equation was $0.82X$ ($p < 0.0001$, $R^2 = 0.88$).

Even though the tracer order of the scans was random and with varying time interval between scans, we conducted a two-way ANOVA on the influence of scan order and tracer on the neocortical BP_{ND}. The effect of tracer yielded an F ratio of $F(1, 8) = 8{,}88$, $p = 0.018$ accounting for 46.78% of the variance, while scan order yielded an F ratio of $F(1, 8) = 0.0062$, $p = 0.94$ and thus was not a significant factor.

Radiometabolism and blood distribution

Both [^{11}C]Cimbi-36 and [^{11}C]Cimbi-36_5 metabolized rapidly (Figure 3(c) and (d)). As previously shown, [^{11}C]Cimbi-36 generated two radiolabeled metabolites identified in plasma; chromatograms (Figure 3(a)) showed an unretained polar fraction (M1), and a less polar fraction (M2). The M2 fraction was significantly larger than the M1 fraction from 10 to 90 min after injection ($p < 0.0004$, Bonferroni-corrected multiple t-tests). In contrast, [^{11}C]Cimbi-36_5 yielded only the M1 fraction (Figure 3(b)).

In addition to the difference in radiometabolite profiles for the two labeling positions, the radioactivity distribution in the blood also differed. The ratio of radioactivity concentration in plasma relative to whole blood was higher for the [^{11}C]Cimbi-36 scans compared with the [^{11}C]Cimbi-36_5 scans (Figure 4). The difference between the means was highly significant from 10 to 90 min after injection ($p < 0.0046$, Bonferroni-corrected multiple t-tests), when more than half of the radioactivity in plasma could be attributed to the radioactive metabolites, whereas 1–5 min after injection, when most of the radioactivity was still in the form of the parent compound, there was

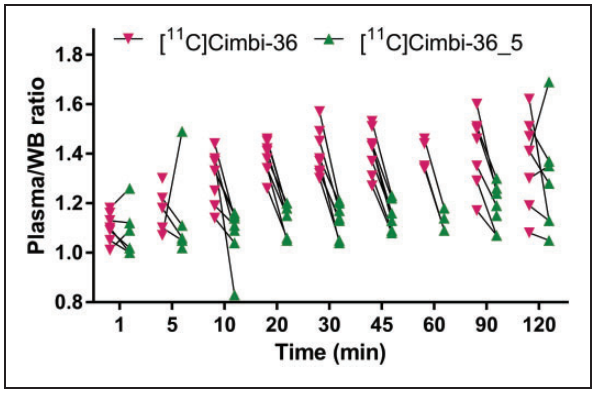

Figure 4. Ratio of radioactivity concentration in plasma relative to whole blood (WB) for [^{11}C]Cimbi-36 ($n = 8$) and [^{11}C]Cimbi-36_5 ($n = 7$).

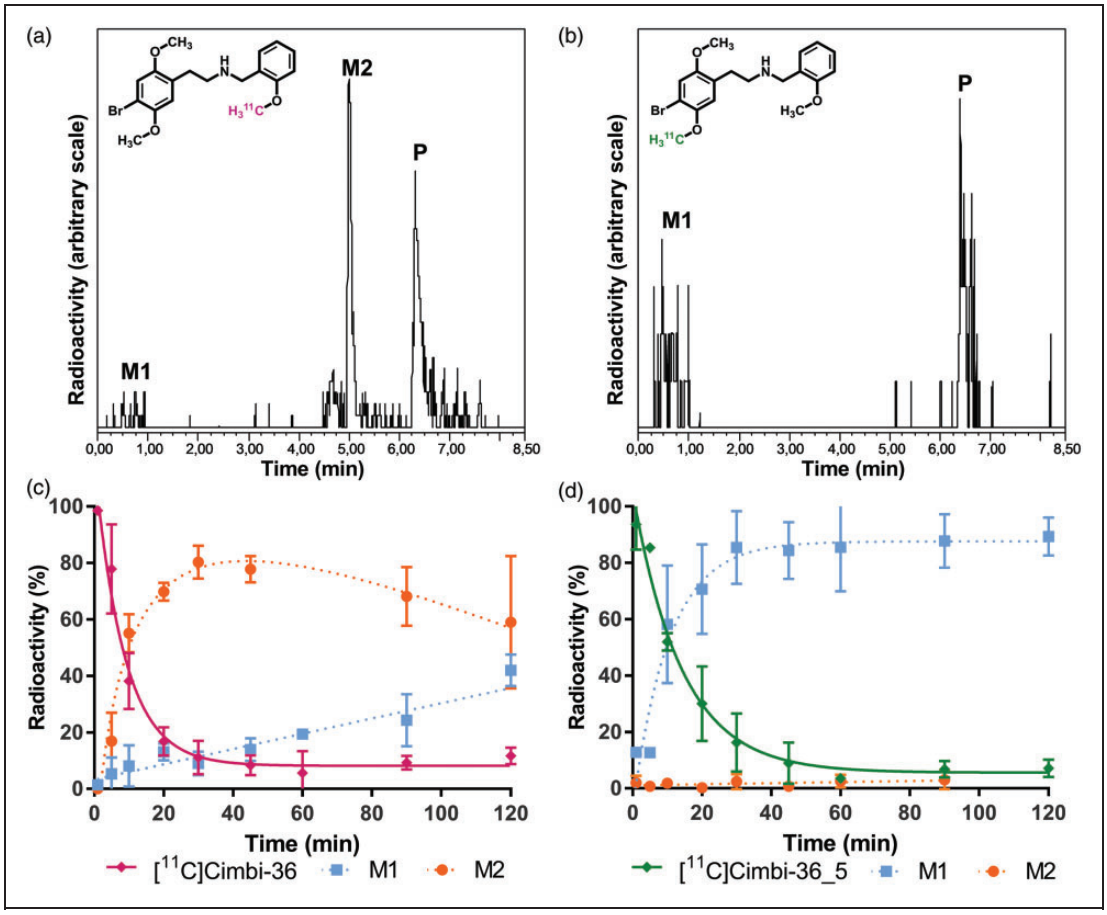

Figure 3. Radio-HPLC analysis of plasma samples 10 min after injection of [^{11}C]Cimbi-36 (a) and [^{11}C]Cimbi-36 _5 (b). Peaks: M1 – polar radiometabolites, M2 – 5′-*O*-glucuronide, P – parent compound. Plasma radiometabolite profiles for [^{11}C]Cimbi-36 (c) and [^{11}C]Cimbi-36_5 (d) throughout the scan (means ± SD).

no statistical difference ($p > 0.64$). At 120 min, the difference also was not significant ($p = 0.40$).

Discussion

Changing the [^{11}C]-labeling position of the 5-HT_{2A}R agonist PET tracer, [^{11}C]Cimbi-36, profoundly altered several key outcome parameters including not just the radiometabolite profile and radioactivity distribution in the blood, but also brain uptake and binding potentials. The BP_{ND} for [^{11}C]Cimbi-36_5 constituted only 82% of the BP_{ND} for [^{11}C]Cimbi-36, which, together with the higher uptake in the cerebellum for [^{11}C]Cimbi-36_5, suggests that the non-displaceable binding is higher for [^{11}C]Cimbi-36_5 than for [^{11}C]Cimbi-36. Since the order of the [^{11}C]Cimbi-36 and [^{11}C]Cimbi-36_5 scans did not influence the BP_{ND} as shown by a two-way analysis, the difference cannot be not explained by carry-over effects from the first scan, particularly as the interval between scans ranged from 3 h to 30 days. The test-retest reproducibility of [^{11}C]Cimbi-36 using the SRTM is high for high binding regions (absolute difference of 3.8% for neocortex[11]), and thus this large difference also cannot be explained by mere test-retest variability.

We propose that the difference in BP_{ND} is caused by penetration of the BBB by the polar M1 radiometabolite fraction. The M1 fraction results from *O*-demethylation and is the major radiometabolite component of [^{11}C]Cimbi-36_5 (5′-*O*-demethylation), but only makes up a smaller fraction of [^{11}C]Cimbi-36 radiometabolites, as the non-labeled 5′-position is preferentially demethylated followed by rapid glucuronidation.[7] The resulting glucuronide radiometabolite appears to be much more stable in vivo, so that only a small fraction of polar (M1) radiometabolites is formed (Figure 3(c)).

O-demethylation of the [^{11}C]-labeled methyl group most likely results in formation of [^{11}C]formaldehyde, [^{11}C]formic acid and/or [^{11}C]carbon dioxide/bicarbonate (Figure 5), as the Cimbi-36 molecule is metabolized by hydrogen abstraction by cytochrome P450 enzymes.[12,13] Although formaldehyde is a highly polar molecule, just like carbon dioxide, it is a small molecule and can therefore cross the BBB[14–17] and other cell membranes. In rats, (R-)[^{11}C]verapamil resulted in formation of [^{11}C]carbon dioxide and other polar radiometabolites, which were subsequently detected in brain tissue.[18] Polar radiometabolites were found in human plasma as well, and proposed to constitute [^{11}C]-labeled formaldehyde, formic acid and carbon dioxide.[19] Studies with [^{18}F]-labeled compounds also show formation of polar radiometabolites, proposed to be [^{18}F]-labeled alcohols, aldehydes and carboxylic acids, which also cross the BBB to some degree.[20,21] In a recently published study, Gustafsson et al.[17] showed that [^{11}C]formaldehyde (and/or its metabolites) and [^{11}C]carbon dioxide/bicarbonate enter the brain following intravenous infusion in rats. In the case of [^{11}C]formaldehyde, the wash-out rate in the brain was slower than in blood, pointing to transformation into other brain-penetrating metabolites and/or retention of formaldehyde itself in the brain. The study also detected [^{11}C]carbon dioxide/bicarbonate in the blood following infusion of *N-methyl*-[^{11}C]oxycodone, which undergoes *N*-demethylation of the radiolabeled methyl group. A similar study could be conducted in pig and human, as the tracer doses used for PET scans would be well below toxic levels.

Our interpretation is further supported by the finding of a significantly lower ratio of radioactivity concentration in plasma relative to whole blood for [^{11}C]Cimbi-36_5 compared with [^{11}C]Cimbi-36 for the timepoints, where the M2 fraction was significantly larger than the M1 fraction (Figure 4). [^{11}C]formaldehyde would likely enter erythrocytes by way of passive diffusion, while [^{11}C]formic acid would mainly stay in the plasma phase, as it would be in its protonated form at physiological pH. [^{11}C]carbon dioxide also passively diffuses into erythrocytes, where some of it would be bound to hemoglobin, while another part would be converted into [^{11}C]bicarbonate that is then transported back into the plasma phase by the Cl-HCO_3 exchanger in the membrane. Although penetration of erythrocytes by part of the M1 radiometabolites is different from penetration of the BBB, it testifies to a clear difference in physical properties of the radiolabeled entities resulting from the two labeling positions, and is in accordance with our interpretation. Similar results are seen for the α_{2c}-adrenoreceptor radioligand, [^{11}C]ORM-13070; polar radiometabolites resulting from demethylation penetrate human erythrocytes[22] and the BBB in mice.[23]

Once the M1 radiometabolites have crossed the BBB they could either return to the blood, get trapped as, e.g. bicarbonate or bind to cellular proteins (a well known property of formaldehyde). Alternatively, the M1 radiometabolites could be taken up by neurons or glia cells and metabolized/incorporated into new molecules. We also cannot completely rule out that metabolism of the parent tracer takes place within the brain, although we would expect the capacity for metabolism to be considerably lower than in the liver. Also, the significantly longer time to peak SUV for [^{11}C]Cimbi-36_5 points to a prolonged build up in neocortex compared with [^{11}C]Cimbi-36, which we attribute to the gradual increase in M1 radiometabolite concentration in plasma and brain throughout the scan.

Looking at equation (1),[24] defining BP_{ND} in terms of distribution volumes (defined as concentration of radioactivity (ideally only the radioligand) in tissue relative

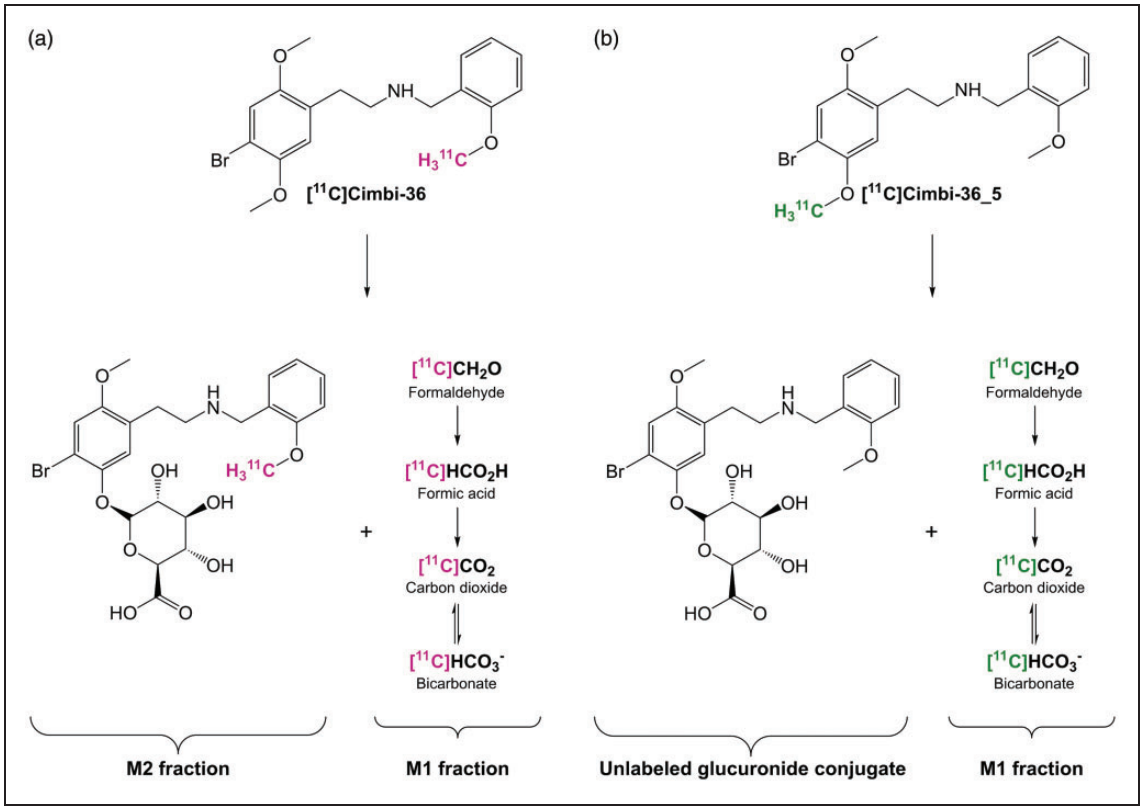

Figure 5. Proposed radiometabolism of [^{11}C]Cimbi-36 (a) and [^{11}C]Cimbi-36_5 (b).

to that in plasma at equilibrium), it becomes clear how increased radioactivity uptake due to increase in radiometabolites entering the brain, can result in decreased BP_{ND} (and vice versa): Given the distribution volume of brain penetrant radiometabolites (V_M) only adds to the distribution volume of nondisplaceable binding ($V_{ND} = V_{free} + V_{non\text{-}specific}$), and enter the target region and reference tissue equally, we see that the numerator remains constant, while the denominator changes with a change in distribution volume of radiometabolites (ΔV_M) (2).

$$\begin{aligned} BP_{ND} &= \frac{V_T - V_{ND}}{V_{ND}} \\ &= \frac{\left\{ \begin{array}{l} (V_{specific} + V_{free} + V_{non-specific}) \\ -(V_{free} + V_{non-specific}) \end{array} \right\}}{V_{free} + V_{non-specific}} \\ &= \frac{V_{specific}}{V_{free} + V_{non-specific}} \end{aligned} \quad (1)$$

$$\begin{aligned} BP_{ND}(\Delta V_M) &= \frac{(V_T + \Delta V_M) - (V_{ND} + \Delta V_M)}{V_{ND} + \Delta V_M} \\ &= \frac{V_T - V_{ND}}{V_{ND} + \Delta V_M} \end{aligned} \quad (2)$$

Instead of adding (or subtracting) an absolute value of ΔV_M, we can express the change in relative terms with a factor, k_M

$$\begin{aligned} k_M = \frac{V_{ND} + \Delta V_M}{V_{ND}} = 1 + \frac{\Delta V_M}{V_{ND}} \Leftrightarrow \\ V_{ND} + \Delta V_M = k_M \times V_{ND} \end{aligned} \quad (3)$$

This we can use to rewrite equation (2)

$$BP_{ND}(k_M) = \frac{V_T - V_{ND}}{V_{ND} \times k_M} = \frac{V_T - V_{ND}}{V_{ND}} \times \frac{1}{k_M} \quad (4)$$

and then we can calculate the relative change in BP_{ND} (ΔBP_{ND}) as a function of k_M

$$\begin{aligned} \Delta BP_{ND}(k_M) &= \frac{BP_{ND}(k_M) - BP_{ND}}{BP_{ND}} \\ &= \frac{\left(\frac{V_T - V_{ND}}{V_{ND}} \times \frac{1}{k_M}\right) - \left(\frac{V_T - V_{ND}}{V_{ND}}\right)}{\frac{V_T - V_{ND}}{V_{ND}}} \\ &= -1 + \frac{1}{k_M} = -1 + k_M^{-1} \end{aligned} \quad (5)$$

This equation is visualized in Figure 6.

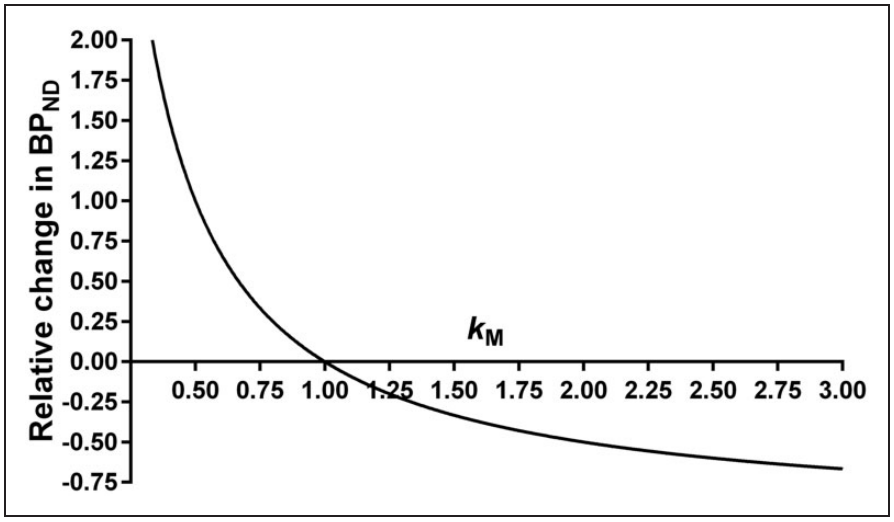

Figure 6. Graphical representation of equation (5): $\Delta BP_{ND} = -1 + k_M{}^{-1}$. Seeing as ΔV_M can have a negative value, k_M can be <1, resulting in an increase in BP_{ND}.

The study is not without limitations and in particular, we did not collect arterial blood samples but only venous samples. Compared with our previous [^{11}C]Cimbi-36 human study,[5] we find here that the M2 radiometabolite constitutes a larger fraction compared to the M1 fraction, and we speculate that this difference emerges as a consequence of blood passing through the tissue capillaries; the polar, yet penetrable M1 radiometabolites would be extracted to some degree by diffusing both para- and transcellularly, making up a smaller fraction in venous plasma. The M2 radiometabolite (5′-*O*-glucuronide conjugate, Figure 5(a)) would instead remain in the plasma or be extracted to a much lesser degree, due to its molecular size, thus making up a larger fraction than in arterial plasma.

Although carbon dioxide is continuously expired, formation of [^{11}C]carbon dioxide/bicarbonate cannot be disregarded in PET studies, as some of it will be trapped in the tissue compartments.[15,17,25] Accordingly, differences in pH and carbon dioxide/bicarbonate between arterial and venous blood may also have an impact, although it is difficult to predict the direction and order of magnitude of these effects. Moreover, if [^{11}C]carbon dioxide/bicarbonate is produced and escapes before the radio-HPLC analysis, the parent fraction and M2 fraction will be overestimated. Thus, if anything, the use of venous rather than arterial samples would tend to underestimate the effects of the polar radiometabolites on receptor measurements. Employing the method used by Gustafsson et al.[17] for [^{11}C]carbon dioxide/bicarbonate detection in future [^{11}C] Cimbi-36 projects would be a simple way to quantify and confirm our interpretation.

Many [^{11}C]-labeled radioligands result in polar radiometabolites, as methylation is a convenient approach for radiosynthesis, but the nature and the impact of these radiometabolites have rarely been investigated. Radiolabeling of a ligand in different positions constitutes a unique possibility for investigating the metabolic fate of the radioligand, and [^{11}C]Cimbi-36 is one of very few radioligands that can be easily radiolabeled in more than one position. It has previously been shown that when [^{11}C]raclopride is radiolabeled in the methyl-position compared to the carbonyl,[26] no difference in BP_{ND} or radiochromatograms is seen. In contrast, [^{11}C]WAY-100635 labeled in the carbonyl position, rather than the methyl, yielded a higher signal-to-background ratio,[27] likely because of the absence of a radiometabolite with high affinity for the target receptor. But even if polar radiometabolites cannot be avoided, or are preferred to radiometabolites with high-affinity for the target, inter-individual differences in metabolic rate or pathways (caused by e.g. genetic variability, pathologic condition or drug intervention), could lead to different levels of polar radiometabolites, which in turn could confound receptor measurements.

Conclusion

Our findings demonstrate that small polar radiometabolites can enter the brain and contribute significantly to non-specific binding. Thus, the assessment as to whether radiometabolites might cross the BBB cannot rely solely on radio-HPLC chromatograms; chemical identity and metabolic rate need to be considered as well. When designing PET studies, factors that could

influence radiometabolism, whether they be related to the test subjects or interventions, should be identified and controlled for if possible.

Furthermore, we conclude that [^{11}C]Cimbi-36 continues to be the tracer of choice for future 5-HT_{2A} receptor agonist studies as it has a lower non-specific binding than [^{11}C]Cimbi-36_5, and thus will be more sensitive to changes in 5-HT_{2A} receptor levels in the brain.

Funding

The author(s) disclosed receipt of the following financial support for the research, authorship, and/or publication of this article: This study was financially supported by the Lundbeck Foundation, the Toyota Foundation and the John and Birthe Meyer Foundation.

Acknowledgements

Technical assistance of Lone Ibsgaard Fryer, Bente Dall, Svitlana Olsen, Gerda Thomsen, Erik Perfalk and Martin Korsbak Madsen is greatly acknowledged.

Declaration of conflicting interests

The author(s) declared no potential conflicts of interest with respect to the research, authorship, and/or publication of this article.

Authors' contributions

HDH, GMK, SL, SLP, JLK and NG jointly developed the setup for the study. AJ performed the scans with assistance from HDH, SL and NG. AJ performed the processing of the data with assistance from CS, and drafted the initial manuscript and performed the literature review. All authors contributed to the discussion of the findings and its implications. All authors reviewed the choice of references and figures, and edited the initial draft and every subsequent draft. All authors approved the final manuscript.

References

1. Pike VW. PET radiotracers: crossing the blood-brain barrier and surviving metabolism. *Trends Pharmacol Sci* 2009; 30: 431–440.
2. Van de Bittner GC, Ricq EL and Hooker JM. A philosophy for CNS radiotracer design. *Acc Chem Res* 2014; 47: 3127–3134.
3. Tonietto M, Rizzo G, Veronese M, et al. Plasma radiometabolite correction in dynamic PET studies: insights on the available modeling approaches. *J Cereb Blood Flow Metab* 2016; 36: 326–339.
4. Ettrup A, Hansen M, Santini MA, et al. Radiosynthesis and in vivo evaluation of a series of substituted 11C-phenethylamines as 5-HT2A agonist PET tracers. *Eur J Nucl Med Mol Imaging* 2011; 38: 681–693.
5. Ettrup A, da Cunha-Bang S, McMahon B, et al. Serotonin 2A receptor agonist binding in the human brain with [11C]Cimbi-36. *J Cereb Blood Flow Metab* 2014; 34: 1188–1196.
6. Halberstadt A. Pharmacology and toxicology of N-benzylphenethylamine (''NBOMe'') hallucinogens. *Curr Top Behav Neurosci* 2017; 32: 283–311.
7. Leth-Petersen S, Gabel-Jensen C, Gillings N, et al. Metabolic fate of hallucinogenic NBOMes. *Chem Res Toxicol* 2016; 29: 96–100.
8. Sureau FC, Reader AJ, Comtat C, et al. Impact of image-space resolution modeling for studies with the high-resolution research tomograph. *J Nucl Med* 2008; 49: 1000–1008.
9. Ganz M, Feng L, Hansen HD, et al. Cerebellar heterogeneity and its impact on PET data quantification of 5-HT receptor radioligands. *J Cereb Blood Flow Metab* 2017; 37: 3243–3252.d.
10. Gillings N. A restricted access material for rapid analysis of [11C]-labeled radiopharmaceuticals and their metabolites in plasma. *Nucl Med Biol* 2009; 36: 961–965.
11. Ettrup A, Svarer C, McMahon B, et al. Serotonin 2A receptor agonist binding in the human brain with [11C]Cimbi-36: test–retest reproducibility and head-to-head comparison with the antagonist [18F]altanserin. *Neuroimage* 2016; 130: 167–174.
12. Caspar AT, Brandt SD, Stoever AE, et al. Metabolic fate and detectability of the new psychoactive substances 2-(4-bromo-2,5-dimethoxyphenyl)-N-[(2-methoxyphenyl)methyl]ethanamine (25B-NBOMe) and 2-(4-chloro-2,5-dimethoxyphenyl)-N-[(2-methoxyphenyl)methyl]ethanamine (25C-NBOMe) in human and rat u. *J Pharm Biomed Anal* 2017; 134: 158–169.
13. Boumrah Y, Humbert L, Phanithavong M, et al. In vitro characterization of potential CYP- and UGT-derived metabolites of the psychoactive drug 25B-NBOMe using LC-high resolution MS. *Drug Test Anal* 2016; 8: 248–256.
14. Raichle ME, Eichling JO, Straatmann MG, et al. Blood-brain barrier permeability of 11C-labeled alcohols and 15O-labeled water. *Am J Physiol* 1976; 230: 543–552.
15. Shields AF, Graham MM, Kozawa SM, et al. Contribution of labeled carbon dioxide to PET imaging of carbon-11-labeled compounds. *J Nucl Med* 1992; 33: 581–584.
16. Shcherbakova LN, Tel'pukhov VI, Trenin SO, et al. Permeability of the blood-brain barrier for intravascular formaldehyde. *Bull Exp Biol Med* 1986; 102: 1553–1554.
17. Gustafsson S, Eriksson J, Syvänen S, et al. Combined PET and microdialysis for in vivo estimation of drug blood-brain barrier transport and brain unbound concentrations. *Neuroimage* 2017; 155: 177–186.
18. Luurtsema G, Molthoff CFM, Schuit RC, et al. Evaluation of (R)-[11C]verapamil as PET tracer of P-glycoprotein function in the blood-brain barrier: kinetics and metabolism in the rat. *Nucl Med Biol* 2005; 32: 87–93.
19. Lubberink M, Luurtsema G, van Berckel BNM, et al. Evaluation of tracer kinetic models for quantification of P-glycoprotein function using (R)-[11C]verapamil and PET. *J Cereb Blood Flow Metab* 2007; 27: 424–433.

20. Luurtsema G, Schuit RC, Takkenkamp K, et al. Peripheral metabolism of [18F]FDDNP and cerebral uptake of its labelled metabolites. *Nucl Med Biol* 2008; 35: 869–874.
21. Zoghbi SS, Shetty HU, Ichise M, et al. PET imaging of the dopamine transporter with 18 F-FECNT: a polar radiometabolite confounds brain radioligand measurements. *J Nucl Med* 2006; 47: 520–527.
22. Luoto P, Suilamo S, Oikonen V, et al. 11C-ORM-13070, a novel PET ligand for brain α2C-adrenoceptors: radiometabolism, plasma pharmacokinetics, whole-body distribution and radiation dosimetry in healthy men. *Eur J Nucl Med Mol Imaging* 2014; 41: 1947–1956.
23. Arponen E, Helin S, Marjamäki P, et al. A PET tracer for brain α2C adrenoceptors, 11C-ORM-13070: radiosynthesis and preclinical evaluation in rats and knockout mice. *J Nucl Med* 2014; 55: 1171–1177.
24. Innis RB, Cunningham VJ, Delforge J, et al. Consensus nomenclature for *in vivo* imaging of reversibly binding radioligands. *J Cereb Blood Flow Metab* 2007; 27: 1533–1539.
25. Gjedde A. Labeled carbon dioxide: how transient a metabolite? *J Nucl Med* 1992; 33: 585–586.
26. Rahman O, Takano A, Amini N, et al. Synthesis of ([11C]carbonyl)raclopride and a comparison with ([11C]methyl)raclopride in a monkey PET study. *Nucl Med Biol* 2015; 42: 893–898.
27. Osman S, Lundkvist C, Pike VW, et al. Characterisation of the appearance of radioactive metabolites in monkey and human plasma from the 5-HT(1A) receptor radioligand, [carbonyl-11C]WAY- 100635 – explanation of high signal contrast in PET and an aid to biomathematical modelling. *Nucl Med Biol* 1998; 25: 215–223.